POLITECNICO
MILANO 1863

SCUOLA DI INGEGNERIA INDUSTRIALE
E DELL'INFORMAZIONE

Executive Summary of the Thesis

Distributed Electric Propulsion Applied to Micro Aerial Vehicles

Laurea Magistrale in Aeronautical Engineering - Ingegneria Aeronautica

Author: Davide La Ferla

Advisor: Prof. Alex Zanotti

Co-advisor: Roberto Albertani, Associate Professor (Ret.)

Academic year: 2024-2025

1. Introduction

Micro Aerial Vehicles (MAV) were originally defined as a category of aircraft with the maximum dimension of 150 mm, a mass of 50 g or less and capable of operating at speeds of 10 m/s. At MAV's operational Reynolds numbers of 50,000 or lower, conventional airfoils experience a significant degradation in aerodynamic performance. Thin zero-thickness airfoils that are employed to mitigate the drop of performance, significantly decrease the vehicle's payload capabilities [1, 2]. Recently developed distributed propulsion (DP), in particular Distributed Electric Propulsion (DEP) was applied on conventional aircraft to improve their aerodynamic characteristics at lower flight velocities [3]. This work focused primarily on the development of an original capability to investigate a novel application of DEP to MAVs aimed at improving the performance of conventional airfoils at low and very-low Re numbers. Wind tunnel testing was performed at Politecnico di Milano using a six-axis micro-sting balance for force and moments estimates. The numerical investigation was carried out using DUST, a particle–panel solver, augmented by Xfoil, NeuralFoil, and SU2 for detailed airfoil analyses.

2. Experimental Setup

Due to the originality of this work, including the lack of any existing reference, the general shape of the model was selected as a rectangular wing planform. An Eppler E231 airfoil was selected, as it offers better lift-to-drag ratio at low Re numbers for the same thickness with respect to the NACA0012. The wing has a span of 200 mm with a chord of 40 mm, which results in an aspect ratio of 5. An elliptical fuselage was added in the center of the wing as the joint for the sting balance. Along the span, the nacelles for the six motors, and relative propellers, are present, one every 33 mm. This meant that the entire wing would be under the influence of the propellers' slipstream, as DP systems would require.

For the model under consideration, the aerodynamic chord, the balance axis, and the motor–propeller axis are mutually aligned and coincide with the 0° angle of attack reference of the model.

The DEP consisted in a series of six commercially available DC motors with their propellers obtained from a Cheerson CX-10 commercial toy drone. Each motor measured 12 mm in length and 6 mm in diameter. The propellers had a diameter of 30.4 mm and the space between each propeller's blade tip resulted in 2.6 mm.

For easing motors installation, since they are thicker than most of the airfoil, the model was divided into 5 parts. All components were designed in Solidworks, 3D printed and then bonded together once the wiring of the motors was done. To fully couple the model and the sting balance, a circular cylinder extrusion and a 3.5 mm diameter hole for the dowel pin were introduced in the fuselage beyond the trailing edge.
The experiments for this project were run at the academic wind tunnel facility at the Politecnico di Milano.
For the proper installation of the model mechanically connected with the sting balance with their centerline aligned with the centerline of the wind tunnel, a custom metal support was designed and manufactured, together with a 3D printed support which also served as the reference surface for 0° angle of attack (AOA) alignment.
The test rig was externally connected to a Parker BE231DQ-NPSN servo motor, through a Parker PX60-040-S2-MU60-033 inline helical planetary gearmotor, to ensure high-accuracy and high-repeatability control of the model's AOA.
To achieve the desired rotational speeds the supply voltage was increased to 7 V, thanks to a KERT KAT10VD power supply. For fine tuning, each motor was connected in series with a PWM, enabling more precise adjustment of the operating conditions. During tests, the rotational speed was obtained through the autocorrelation of the signal coming from the balance normal axis component. The experimental procedure included that the angle of attack order was randomized to avoid the risk of systematic errors influencing the results.
The full model manufactured is shown in Fig. 1.

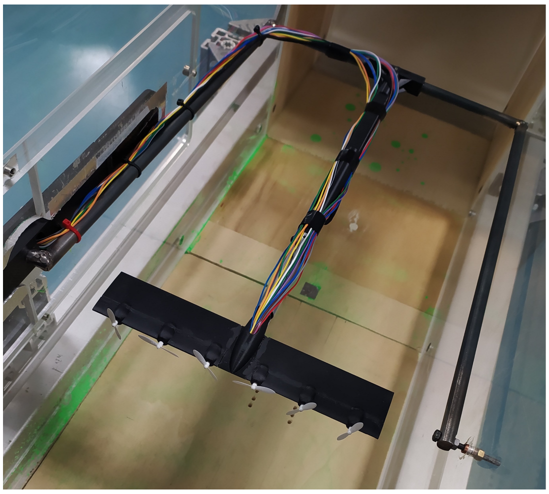

Figure 1: Lift coefficient at different freestream velocities.

To measure the loads generated by the wind tunnel model, the Modern Machine & Tool CO., INC. *MC.-10-.375 Balance*, was used. Data acquisition and processing were based on a LabVIEW VI suite. The sampling was performed by averaging the signal of the transducers with a 25 kHz frequency, for 4 seconds.
The calibration matrix given by the sting balance factory resulted erroneous once it was tested with known loads applied, thus the calibration procedure was repeated. Given the complexity of a full calibration on all six axes, just the three axes of interest in this study were re-calibrated, namely axial force (AF), normal force (NF) and pitching moment (PM). A custom calibration support was also designed and manufactured. The convention for signs of forces and moments respected the indication of positive normal force upwards described in the balance technical drawings, while the axial force was chosen positive inward, to signify drag. Finally, the pitching moment was chosen as positive for the pitch-up direction.

3. Numerical Analysis

To estimate the loads acting on the model, a series of numerical simulations have been carried out, using primarily the DUST software, with the aid of Xfoil, the NeuralFoil python library and SU2 to validate the results.
The Xfoil analysis of the E231 airfoil at this very low Reynolds number predicted stall at all angles of attack. Because Xfoil's reliability in such low-Reynolds conditions was questionable, higher-fidelity RANS CFD simulations were subsequently performed using SU2 to obtain more accurate results. The free-stream velocity was set to 10 m/s. The parameters for the boundary layer construction were chosen to achieve a wall $y^+ \simeq 1$. A grid convergence study was performed to prove the robustness of the results and to choose the proper mesh to apply in the simulations, with the final choice of a 57965 nodes mesh.

The result of the simulation was compared with the experimental result in Table 1.

Alpha	C_L SU2	C_L exp.	Δ C_L%
0°	0.1903	0.2060±0.002	-7.6

Table 1: Comparison for lift coefficient, with relative error, between SU2 simulations and experimental results.

The setup was defined with the objective of minimizing the error in the lift coefficient at 0° angle of attack; consequently C_D and relative error was neglected. The SU2 analysis showed that the profile was not stalled and consequently Xfoil analysis is not to be trusted for the prediction of aerodynamic coefficients at very low Reynolds for thick airfoils.
DUST is an open-source software developed by Politecnico di Milano that solves different aerodynamic problems with a mid-fidelity approach. Through a spatial sensitivity analysis, the wing was modeled with 50 spanwise points of a lifting line, each of which had the relative airfoil performance given by the experimental results. The propeller was also modeled as a lifting line, to capture viscous phenomena and to limit computational time. The aerodynamic characteristics of the airfoil were inputted by NeuralFoil tabulated data, since the latter's capabilities for thin profiles were attested. A sensitivity analysis was conducted for both spatial and time discretization. The propeller blade was discretized in 15 panels in the spanwise direction. A temporal discretization corresponding to 40 time steps per propeller revolution was selected.
The full model constituted in the wing upstream of the propeller at an angle of attack of 7.5°, a freestream velocity of 5 and 10 m/s and a rotational speed of 60000 RPM.

4. Results and discussion

The beginning of the experimental campaign in the wind tunnel was designed to provide the baseline with the clear wing at the Reynolds reported in Table 2.
Lift, drag (through polar) and pitch moment coefficients, at various Re numbers, are presented in Figs. 2, 3, 4.

Speed	Dynamic Pressure	Re
5 m/s	14.6 Pa	13235
7.5 m/s	33.1 Pa	19853
10 m/s	62.0 Pa	26471
15 m/s	132.6 Pa	39706

Table 2: Wing's Re numbers based on the chord and dynamic pressure for the airspeed settings of the wind tunnel.

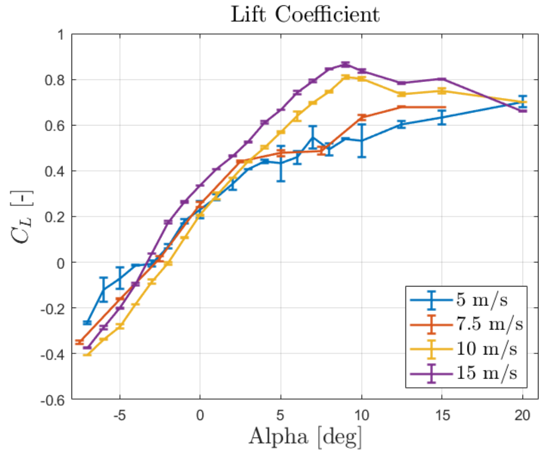

Figure 2: Lift coefficient at different freestream velocities.

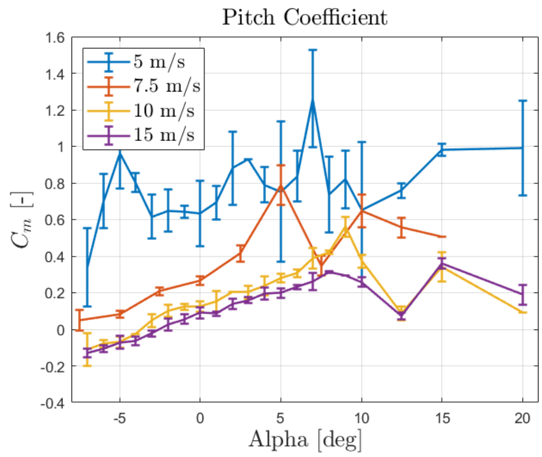

Figure 3: Pitch moment coefficient at different freestream velocities.

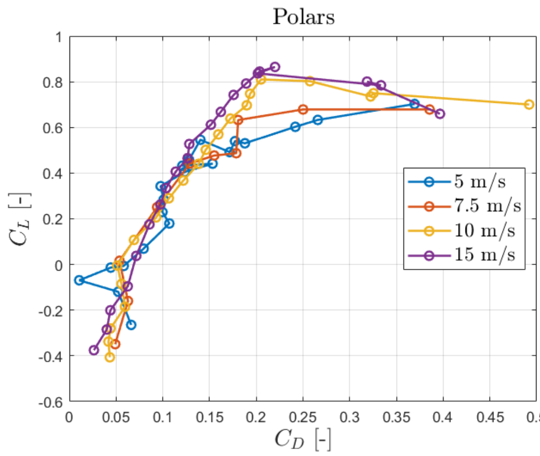

Figure 4: Polar curves at different freestream velocities.

C_L exhibits an increase in the stall angle from about 5° to 10°at higher Re numbers. The pitching moment coefficient exhibits a highly non linear behavior, more apparent at lower velocities. As the velocity increases, the polars exhibit a more conventional aerodynamic behavior. The increase in stall angle of attack is also reflected in a higher maximum L/D value, which rises from 3.5 at 5 m/s to 4.2 at 15 m/s, and occurs at correspondingly higher values of C_L.
The experimental results were employed to validate the numerical simulations. Fig. 5 shows the comparison of results on the Clear Wing at the freestream velocity of 10 m/s.

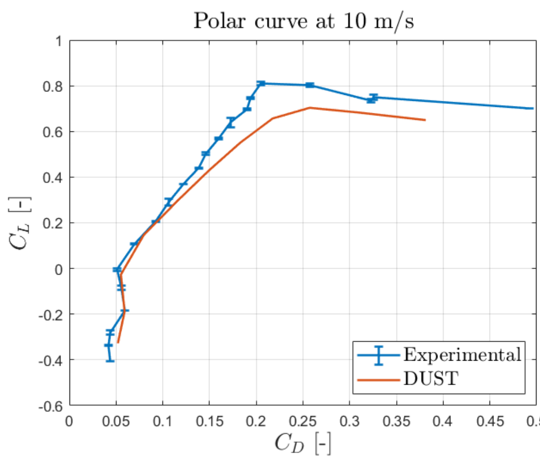

Figure 5: Polar curve comparison between numerical simulation and experimental results at 10 m/s (Re = 26471) in isolated wing configuration.

The wing on DUST was modeled using the airfoil table derived from the experimental tests, thus the simulation closely matches the experimental results as expected.
The experimental characterization of the propulsion's system started with static thrust measurements of a single propeller with respect to the RPM, followed by the numerical counterpart. The results of multiple runs are shown in Fig. 6, where different colors correspond to different runs, the continuous line represents the best fit of the data obtained using the least-squares method and the numerical results are shown in red. The propeller's pitch angle was set to 13°, since the best agreement with the experimental thrust was sought, and that value provided the closest match.

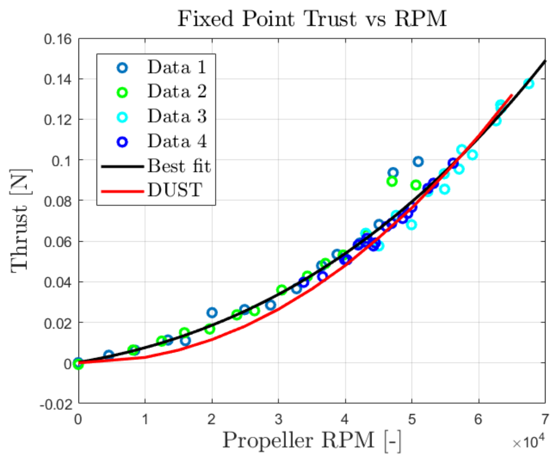

Figure 6: Comparison between numerical and experimental results for the propeller thrust. Input voltage 0 to 7 V for experimental values.

For the rotational speed applied for all wind tunnel tests of 60,000 RPM, simulation and experimental thrust are in perfect agreement.
The experimental campaign proceeded with tests on the complete model. The tests were conducted for a propeller rotational speed of approximately 60000 RPM and for two different airspeeds, 5 and 10 m/s.
In the experimental campaign, unlike in the numerical simulations, it was not possible at this preliminary stage to separate the vertical component of the propeller thrust from the lift increase caused by the wing's performance enhancement due to the propeller blowing effect.
The only case in which the propeller thrust did not influence the lift coefficient was at 0° angle of attack, since the thrust has no vertical component in this condition. This allowed the lift im-

provement due exclusively to the blowing effect to be isolated, excluding any contribution from the thrust itself. Table 3 shows that the blowing effect increases the lift coefficient at both freestream velocities considered.

Velocity	Configuration	C_L	Δ C_L%
5 m/s	Clear Wing Full model	0.2294 0.6014	+162%
10 m/s	Clear Wing Full model	0.2060 0.3787	+83.8%

Table 3: Comparison of wing performance between the Clear Wing and the Full model, for the two freestream velocities analyzed at 0° AOA.

Returning to the numerical approach, simulations were carried out at 7.5° AOA for both velocities analyzed, and the comparison with experimental results is illustrated below.
The numerical approach, once validated, allowed for useful insights in the flow physics and phenomena thanks to DUST post-processing capabilities. First, it was possible to separate the different contributions of the different components toward the global loads. The results of the test are presented in Table 4.
Table 4 shows that the direct contribution of the propellers to the global lift was significantly lower than the contribution due to the wing.
Savino et al. [4] showed that at advance ratios J=0.5 and J=0.75, an interaction mechanism between the propeller tip vortices and the wing wake occurs at higher Reynolds numbers, similar to what happened here at low Reynolds. Specifically, the same increase in vorticity intensity was also observed as the free stream velocity decreased, and a greater improvement in wing performance was observed for the lowest advance ratio, corresponding to the lowest free-stream velocity, where the propeller operates more effectively.
The numerical approach allowed in the wing-propeller complete model the separation of the contribution of the wing and the propellers, thus the difference in aerodynamic performance with the wing without propeller was found. The results are reported in Table 5. It can be clearly observed that DEP provides a substantial improvement in wing lift coefficient with an increase of a factor of approximately four at a freestream of 5 m/s and two at 10 m/s, at the same propeller's rotational speed. The difference can be attributed to the relative influence of the propeller's wake effect which is significantly greater at 5 m/s.
In conclusion, the application of DUST to low Reynolds number flows, while also requiring very small time steps for propeller resolution, leads to numerical oscillations in the wake, thereby reducing the reliability of the results. In the absence of experimental data for validation, the credibility of the numerical solution remains uncertain. Therefore, in its current state, DUST should be regarded primarily as an analysis tool capable of providing qualitative insight into flow phenomena and the underlying physics, once it has been validated against experiments. However, it cannot yet be considered a fully predictive tool for this class of problems.

5. Conclusions

In this project, a novel experimental setup for powered Micro Aerial Vehicles, which included a newly acquired micro six-axes sting balance, was developed at the Politecnico di Milano's small

Velocity	Component	F_y	C_L	%	F_x	C_D	%
5 m/s	Wing	0.2182	1.7812	73.4%	0.1380	1.1265	32.9%
	Propellers	0.0790	0.6449	26.6%	-0.5569	-4.5461	-132.9%
	Full Model	0.2972	2.4261	100%	-0.4189	-3.4196	-100%
10 m/s	Wing	0.5743	1.1720	91%	0.1270	0.2592	49.1%
	Propellers	0.0569	0.1161	9%	-0.3857	-0.7871	-149.1%
	Full Model	0.6312	1.2881	100%	-0.2587	-0.5280	100%

Table 4: Force coefficients in wind axes, divided by component, for the two freestream velocities analyzed.

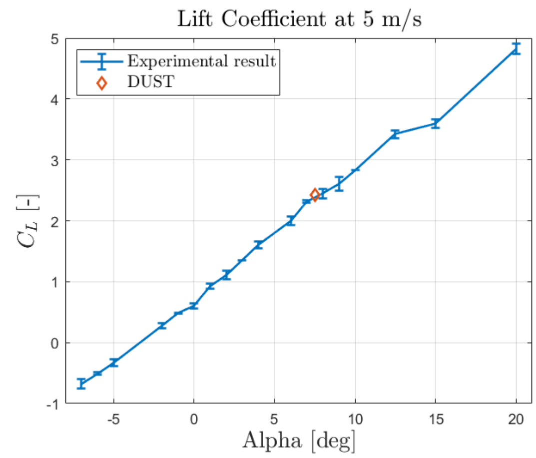

(a) Lift coefficient at 5 m/s, wing's Re = 13235.

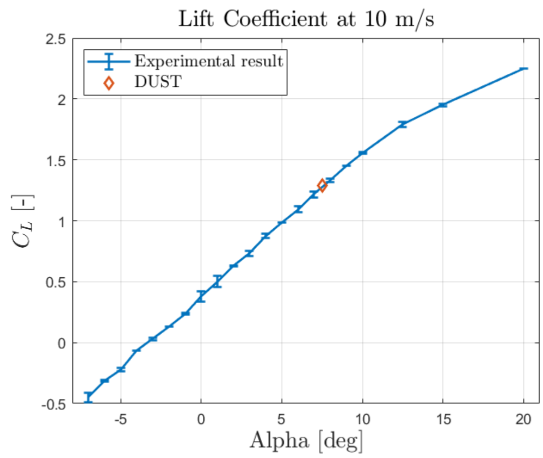

(b) Lift coefficient at 10 m/s, wing's Re = 26471.

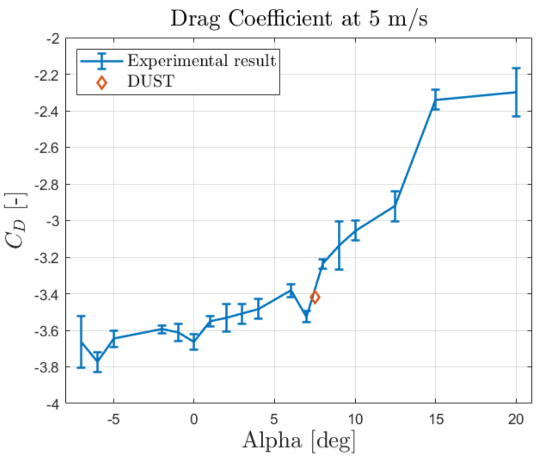

(c) Drag coefficient at 5 m/s, wing's Re = 13235.

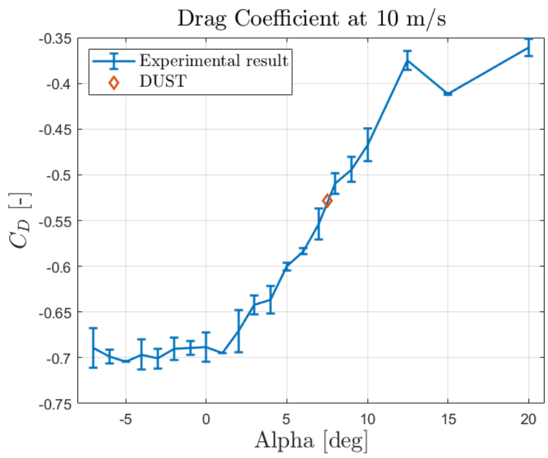

(d) Drag coefficient at 10 m/s, wing's Re = 26471.

Figure 7: Lift and drag coefficients comparison for the full model against experimental results. Propeller speed 60,000 RPM, voltage input 7 V.

academic wind tunnel. A full scale model of a MAV's wing with six motor-propeller units was designed from scratch and manufactured to study the effects of distributed electric propulsion on the wing, together with a custom test rig to mount and aligne the model with. The test rig, completed of the model was validated for accuracy and feasibility of measures at Re between 13 to 40 thousand. The aerodynamic coefficients obtained showed reliable behavior across different Reynolds.
Part of the project consisted in the development of a virtual twin of the wind tunnel model with the objective to validate the numerical simulation analysis. For all components, the numerical analysis showed excellent agreement with experimental testing, proving the capability of DUST to accurately represent the interactional aerodynamics also at such low Reynolds regimes.
The combined experimental and numerical investigation demonstrated a significant increase in wing aerodynamic performance due to the application of DEP.
The experimental results showed that, at zero angle of attack and for a propeller rotational speed of 60000 RPM, the blowing effect produced an increase of 83.8% of C_L at Re=26471, and an increase of 162% at Re=13235.
At a angle of attack of 7.5° and a propellers' speed of 60000 RPM, numerical results showed that lift is primarily wing generated, with wing's C_L increasing by 112.7% at Re=26471 and 303% at Re=13235.
These results show that while the reduced advance ratio enhances lift through stronger slipstream-wing interaction, it also significantly

Velocity	Configuration	C_L	$\Delta\ C_L\%$	C_D	$\Delta\ C_D\%$
10 m/s	Clear Wing Blown wing	0.5509 1.1720	+112.7%	0.1830 0.2592	+41.6%
5 m/s	Clear Wing Blown wing	0.4420 1.7812	+303%	0.1438 1.1265	+683.4%

Table 5: Comparison of wing performance between the Clear Wing and the Full model wing component, for the two freestream velocities analyzed.

penalizes the overall aerodynamic efficiency of the wing, particularly at the lowest Reynolds number investigated.

References

[1] Gabriel Torres. Aerodynamics of low aspect ratio wings at low reynolds numbers with applications to micro air vehicle design /. 09 2002.

[2] Thomas J. Mueller and James D. DeLaurier. Aerodynamics of small vehicles. *Annual Review of Fluid Mechanics*, 35(Volume 35, 2003):89–111, 2003.

[3] Hyun D. Kim, Aaron T. Perry, and Phillip J. Ansell. A review of distributed electric propulsion concepts for air vehicle technology. In *2018 AIAA/IEEE Electric Aircraft Technologies Symposium (EATS)*, pages 1–21, 2018.

[4] Alberto Savino and Alex Zanotti. Aerodynamic interaction between wing and propeller in evtol airplane mode flight condition. *CEAS Aeronautical Journal*, 06 2025.